Properties of Mode-Locked Optical Pulses in a Dispersion-Managed Fiber-Ring Laser Using Semiconductor Optical Amplifier as Active Device

Jacques W. D. Chi, Arnaud Fernandez, Chao Lu

Properties of Mode-Locked Optical Pulses in a Dispersion-Managed Fiber-Ring Laser Using Semiconductor Optical Amplifier as Active Device

Jacques W. D. Chi, Arnaud Fernandez, and Chao Lu, *Member, IEEE*

***Abstract*— A hybrid model is proposed in order to exploit the idea of compensating semiconductor optical amplifiers (SOAs) nonlinearity by adjusting cavity dispersion in a SOA-fiber ring mode-locked laser. The model is checked by analytical as well as experimental results. Excellent agreement is obtained in both cases. It is predicted that, once the cavity dispersion is correctly adjusted, the mode-locked pulses of 10 ps width will become distortion-free Gaussians, with their time-bandwidth product (TB) very close to the fundamental Gaussian limit (TB = 1/2) using root-mean-square definition. We will show evidence and explain why other waveforms, notably soliton, are highly unlikely in such a system. Some interesting effects related to band-pass filter are revealed as well. Our results highlight the ambiguity of TB using full-width at half-maximum (FWHM) definition. As a consequence, the widely adopted notion of transform-limited pulse in its FWHM version might be misleading.**

***Index Terms*— Optical pulses, pulse generation, semiconductor fiber ring laser, transform-limited pulse, ultrafast optics.**

I. Introduction

OPTICAL pulses as clean as possible, *i.e.*, distortion-free and containing few chirp in both their time waveform and spectrum, are highly important everywhere they appear. In theoretical studies, notably in mode-locked lasers, models are built assuming ideal waveforms such as Gaussian [1] and soliton [2]. In optical communication networks using time- or wavelength-division multiplexing (TDM or WDM), a clean pulse train increases data transmission capacity by reducing the time slot per bit at a given bandwidth (TDM), or reducing its bandwidth per channel at a given bit-rate (WDM). Therefore, how to obtain a clean optical pulse train fast enough for such applications, and how to measure it, are of remarkable importance and vast implications.

The cleanness of an optical pulse is most objectively and quantitatively measured by its time-bandwidth product (TB) using root-mean-square (RMS) definition, *i.e.*, the standard deviation of energy densities of a signal in the time- and frequency domain. The *Uncertainty Principle* states that TB $\geq$ 1/2, the equality being uniquely obtained with an ideal (chirp-free) Gaussian [1], [3]. For an ideal hyperbolic secant (first-order soliton), we calculated TB = 0.5236. Therefore, if one obtains for sure $0.5 \leq$ TB < 0.5236 for an optical pulse, it cannot be a soliton but might be a chirped Gaussian. In this paper, we will use this method to distinguish a soliton and a Gaussian. In the following, we call TB = 1/2 as the Gaussian limit, and a pulse with TB $\sim$0.5 as a Gaussian-limited pulse, in contrast to a transform-limited pulse [1]. This last one routinely applies to a pulse with $\Delta f \Delta t \sim 0.5$, Δf and Δt being intensity full-width at half-maximum (FWHM) in the frequency- and time domain, respectively. As will be shown and discussed later, it turns out that $\Delta f \Delta t$, and hence the notion of Transform-limited Pulse in FWHM version, are ambiguous and might be misleading. The situation could be even worse if Δt is obtained using autocorrelation technique [4].

In our attempt to achieve clean pulses, we have carried out an experiment using a semiconductor optical amplifier (SOA) and dispersion-compensating fiber (DCF) to form a ring laser [5]. As has been explained in [5], the objective is to compensate SOA's nonlinearity, mainly caused by carrier dynamics, by an appropriate amount of negative dispersion [6]. The resulting actively mode-locked pulses at 10 GHz repetition rate are indeed transform-limited, with $\Delta f \Delta t = 0.46$. In this experiment, noticeably, the pulse's shape is not estimated by autocorrelation plus curve-fitting, but directly observed with a fast optical sampling oscilloscope; the spectrum is obtained using a high-resolution optical spectrum analyzer. This provides an excellent opportunity to test a theoretical model about mode locking, which, once validated, could reply to some interesting questions: 1) What these transform-limited pulses really are? Could they reasonably be approximated by Gaussians or solitons? 2) How close these pulses could be to the fundamental Gaussian limit, once relevant parameters are optimized?

Keeping these questions in mind, we propose and develop the present hybrid model, based on the experiment in [5]. In this model, the SOA's behavior is described and then resolved in the time domain, results are checked by analytical formulas; the transmission out of SOA is calculated in the frequency

Manuscript received August 28, 2012; revised October 24, 2012; accepted November 19, 2012. Date of publication November 29, 2012; date of current version December 17, 2012.

J. W. D. Chi is with Ecole Nationale d'Ingénieurs de Brest, Laboratory RESO/Lab-STICC, Brest 29608, France (e-mail: chi@enib.fr).

A. Fernandez is with LAAS Toulouse, Toulouse Cedex 4 31077, France (e-mail: afernand@laas.fr).

C. Lu is with the Department of EIE, Polytechnic University, Hong Kong (e-mail: enluchao@polyu.edu.hk).

Color versions of one or more of the figures in this paper are available online at http://ieeexplore.ieee.org.

Digital Object Identifier 10.1109/JQE.2012.2230317

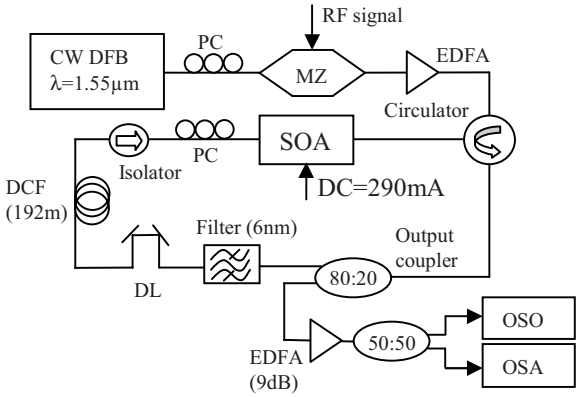

Fig. 1. Experimental setup. MZ: Mach-Zehnder amplitude modulator. PC: polarization controller. DL: delay line. EDFA: erbium-doped fiber amplifier. DCF: dispersion compensating fiber. OSO: optical sampling oscilloscope. OSA: optical spectrum analyzer.

domain. The overall precision is estimated to be $\sim 10^{-4}$ in the evaluation of TB, which is good enough for addressing the above questions.

In Section II, the experiment in [5] and relevant results are briefly reminded for consistency. The hybrid model and the algorithm are developed in Section III, together with comparisons between the model's predictions and available analytical results. In Section IV, the experimental condition is applied to the model so as to directly check its outcome, followed by detailed inspection of optical pulses' properties in similar conditions. Our conclusions are presented in Section V.

II. Experiment

The experimental setup is shown in Fig. 1. In this experiment, the SOA (by CIP, ref. SOA-NL-OEC) as the gain medium exhibits 1 dB polarization gain dependence. It has a multi-quantum-well (10 wells) structure with a length $L_{SOA} =$ 1.5 mm, shows its peak gain at 1555 nm, and provides 28 dB small-signal optical gain at 290 mA DC drive. Its optical gain is periodically modulated at 10 GHz by an optical back-injection. The noise in the ring will circulate clockwise, and eventually grow into mode-locked pulses if conditions are propitious. The band-pass filter serves to locate the carrier frequency, as well as to limit the noise level in the ring cavity. The length of DCF is estimated using a model in [7]. The characteristics of all these components are either provided by their producers, or measured by ourselves [5]. All of them are commercially available. The modulation and the filter functions are also measured and will be given in Section III. The parameters adopted are listed in Table 1.

The average power of the extracted pulse train is $\sim$0.3 mW (with an average back injection power of $\sim$9 mW), its spectral width is less than 1nm. This pulse train is first boosted by an EDFA with +9 dB gain. Compared to EDFA's saturation power ($\sim$10 mW) and its amplification bandwidth (>35 nm) [8], the differences are $1 \sim 2$ orders of magnitude for both values. Therefore, the pulse's original shape and spectrum are preserved after EDFA. The amplified pulse train is then analyzed simultaneously by an optical sampling oscilloscope (OSO, Ando AQ7750), with its input bandwidth

TABLE I
Parameters Used in the Simulation

Symbol	Quantity	Value or Relation
α_H	Henry's factor	6.0
α_{int}	SOAs internal loss	8.86 cm^{-1}
β_0	Wavenumber	$2\pi/\lambda$
B_{BP}	Filter bandwidth	variable, 5−6 nm
E_{sat}	SOAs saturation energy	0.5 pJ
$2\Delta_m$	Modulation index	1.4
D	Dispersion parameter	−139.2 ps/(nm·km) for DCF (to be averaged with SMF)
g_0	Small-signal gain	51.84 cm^{-1} ($G_0 =$ 28 dB net gain)
L_{SOA}	SOAs length	1500 μm
L	Total length of the ring	variable (DL= −10 $\sim$-25 ps/nm)
λ	Wavelength	1.55 μm
ω_0	Carrier frequency	$2\pi c/\lambda$ s^{-1} ($c = 3 \times 10^8$ m/s)
ω_m	Modulation frequency	$2\pi \times 10^{10}$ s^{-1}
v_g	Group velocity in SOA	c/4 m/s
τ	Carrier lifetime	16 ps

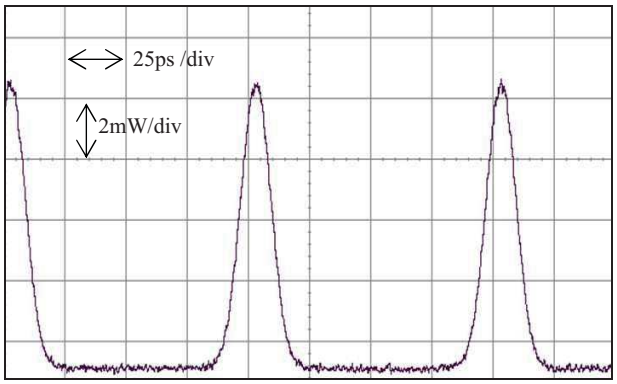

Fig. 2. Oscilloscope trace of the output pulse train.

of 500 GHz and a resolution of 0.6 ps in time, and by an optical spectrum analyzer (OSA, Apex AP2440A), with its spectral resolution of 0.16 pm or 20 MHz between $\lambda = 1520 \sim$ 1567 nm. The peak power in the ring cavity, just before the output coupler, is estimated to be $\approx$12 mW.

The oscilloscope trace of the output pulse train is shown in Fig. 2. These pulses have a FWHM width of $\Delta t \cong 12$ ps. Notice that there are some slight fluctuations around the peaks. The spectrum has been shown in Fig. 2(d) in [5], together with a Gaussian fit. The fitting quality there is excellent. The product $\Delta f \Delta t = 0.46$ is thus obtained. Therefore, these pulses are indeed transform-limited (always in FWHM version).

It should be noticed that the insertion of DCF into the ring cavity is not easy [9], due to structure and material differences between DCF and single-mode fiber (SMF) used for linking different elements. The insertion loss per facet of DCF could

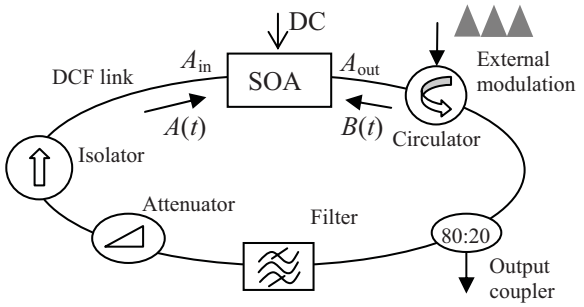

Fig. 3. Schematic of the model.

be as low as −2 dB in our experiment, but that value is far from regularly obtainable. This is the reason why it is difficult, at least for now, to insert a designed length of DCF into the ring laser while maintaining an acceptable insertion loss.

III. Model and Algorithm

A. Hybrid Model

The schematic of the model is depicted in Fig. 3. Recognizing that pulse width $\Delta t \geq 6$ ps in general in SOA-related lasers excluding external pulse compression, it is not necessary in the present model to include the effect of gain dispersion, since its time constant is ∼0.1 ps [10]. Other ultrafast effects, notably two-photon absorption, are also neglected for the same reason and the fact that optical power level is moderate here [11]. In this regime, the dominant physical effects inside SOA are carrier recovery and gain saturation. Assuming slowly-varying envelops, the electrical field in SOA is

$$E(z,t) = [A(z,t)\exp(i\beta_0 z) + B(z,t)\exp(-i\beta_0 z)] \times \exp(-i\omega_0 t). \quad (1)$$

Here, A and B are the forward (+z) and the backward (−z) field envelops, β_0 and ω_0 are the free-space propagation constant and the carrier frequency, respectively. Lateral and polarization effects are ignored. Notice that the carrier frequencies for A and B are independent, but this makes no difference in the model. The propagation for A, B is described by [6], [7]:

$$\partial_z A + v_g^{-1}\partial_t A = \frac{1}{2}[g(1 - i\alpha_H) - \alpha_{\text{int}}]A \quad (2)$$

$$-\partial_z B + v_g^{-1}\partial_t B = \frac{1}{2}[g(1 - i\alpha_H) - \alpha_{\text{int}}]B. \quad (3)$$

Together with the rate equation for the optical gain $g(z,t)$:

$$\partial_t g = \frac{g_0 - g}{\tau} - g\frac{\left(|A|^2 + |B|^2\right)}{E_{sat}}. \quad (4)$$

In the above equations, v_g is the group velocity in SOA, α_H is the Henry's factor, α_{int} is SOA's internal loss coefficient, g_0 is the small-signal optical gain, τ is the carrier lifetime, E_{sat} is the saturation energy. The small-signal net gain is thus $G_0 = \exp[(g_0\text{-}\alpha_{\text{int}})L_{\text{SOA}}]$. Due to a narrow frequency bandwidth involved, these parameters are assumed to be constant. Notice that the noise term is not explicitly present in (2)–(4), it will be included as an additional input afterward.

The SOA's output envelop (A_{out} in Fig. 3) makes a roundtrip through the ring, and emerges as a renewed input A_{in}. The transmission of the pulse train in the fiber link of ∼200 m could be considered as linear, since with a peak intensity of ∼10 mW, the nonlinear length L_{NL} will be ∼50 km for a typical SMF [12]. Therefore, nonlinear effects in the fiber link are not a concern, even though relevant fiber parameters in our experiment differ from those in [12]. Consequently, the transmission through the fiber link could be described by a transfer function in the frequency domain

$$H(\omega) = \frac{\tilde{A}_{\text{in}}^{N+1}(\omega)}{\tilde{A}_{\text{out}}^{N}(\omega)} = \eta \times \exp\left[-\frac{1}{2}\left(2\sqrt[4]{\ln 2}\frac{(\omega-\omega_0)}{B_{\text{BP}}}\right)^4\right] \times \exp\left[i\beta_2 L\frac{(\omega-\omega_0)^2}{2}\right]. \quad (5)$$

Here, $\tilde{A}_{\text{in}}^{N+1}$ and $\tilde{A}_{\text{out}}^{N}$ are the frequency-domain presentations of A_{in}^{N+1} and A_{out}^{N}, respectively, with the integer N denoting the number of roundtrip; η is the total amplitude attenuation, including the loss from the output coupler; B_{BP} is the band-pass filter's 3 dB bandwidth, its flat-top form is checked by us and is well fitted by the first exponent above. For simplicity, we assume that the filter is centered at ω_0. The consequence of this assumption will be discussed later. The second exponent depicts the effect of group velocity dispersion (GVD) in the fiber link, β_2 is the GVD parameter averaged throughout the link, and L is the total length of the ring. In the following, we replace β_2 by the dispersion parameter D through the relation $D = -2\pi c\beta_2\lambda^2$, with $\lambda = 1.55$ μm. Higher-order dispersion is neglected due to relatively long pulse widths and the high value of β_2 involved [12], in consistency with the rest of the model.

Some other components are also implicitly contained in (5). These include a polarization controller, whose attenuation is accounted for by η, and an optical delay for synchronization. It is assumed that harmonic mode-locking is achieved, *i.e.*, the roundtrip delay corresponds to an exact multiple of modulation period. This explains the absence of β_1 (the inverse of the group velocity in the fiber) in (5). In effect, the optical delay in Fig. 1 is already included in the total length L. Mode-locking is achieved if with a big enough N (∼10^2), $|A_{\text{in}}^{N+1}| = |A_{\text{in}}^{N}|$. The hybrid model is thus complete.

B. Algorithm

Since (5) is essentially error-free, the resolution of (2)–(4) determines the precision of the model. In order to achieve high precision, we have upgraded the algorithm in [7] to a higher order. The detailed formulation is available in [13], which adopts a predictor-corrector strategy [14], and is equivalent to the well-known 4$^{\text{th}}$-order Runge-Kutta algorithm in terms of convergence [15]. Notice that the effect of gain dispersion is included in [13] as well, in order to take on optical pulses as short as ∼1 ps in future studies.

To adapt the above algorithm to the experiment in Fig. 1, the modulation period is divided into 2^M equal intervals (256 to begin with, up to 4096 to ensure convergence and precision). For a 10 GHz signal, this corresponds to a stepsize of $\delta t =$

$100/2^M$ [ps]. The SOA is divided accordingly, with a space division $\delta z = v_g \delta t$.

At $t = 0$, a trigger signal $A^0_{\text{in}}(t)$ at the front facet, and the back injection (modulation) signal $B(t)$ at the rear facet, are simultaneously injected into SOA. The trigger A^0_{in} could be a random signal emulating a noise, or simply a sinus $A^0_{\text{in}} = a\sin(bt)$ with arbitrary (a, b), or a combination of both. As a matter of fact, we observed that the final outcomes are independent of the choice of A^0_{in}, as long as this last one has reasonable peak power (at -40 dBm, say). Meanwhile, the modulation signal can be written as [1]

$$B(t) = B_0 \exp\left[-\Delta_m(1 - \cos\omega_m t)\right] \tag{6}$$

where B_0 is the peak amplitude of the modulation envelop, $2\Delta_m$ is the modulation index, and $\omega_m = 2\pi \times 10^{10}$ is the modulation frequency. This function has been verified in [5]. The output envelop $A^0_{\text{out}}(t)$ is then calculated using the algorithm mentioned above. It is converted to $\tilde{A}^0_{\text{out}}\omega)$ by Fourier transform (FT). The next input $A^1_{\text{in}}(t)$ is obtained from

$$A^1_{\text{in}}(t) = FT^{-1}\left[H(\omega)\tilde{A}^0_{\text{out}}(\omega)\right]. \tag{7}$$

A complete roundtrip is thus accomplished. A random noise emulating spontaneous emissions in SOA could be added to A^1_{in}, as well as to the following roundtrips. It is observed, however, that the end results are insensitive to such a noise, as long as its power level is realistic (-40 dBm is applied in our simulations). The only perceptible consequence is a slight fluctuation ($\sim 10^{-4}$) of TB. This observation might be explained by the permanent presence of a large number of coherent photons in SOA. In effect, even at its intensity trough, $|B|^2_{\min} \approx 7.4$ mW (using $B_0^2 = 30$ mW and $\Delta_m = 0.7$), which is far more intense than any possible noise. Therefore, spontaneous emissions could not grow perceptibly (except those photons joining mode-locked pulses) and remain weak enough to be neglected. Consequently, all noises are ignored after the trigger A^0_{in}.

The new input $A^1_{\text{in}}(t)$ is synchronized to $B(t)$ to obtain $A^1_{\text{out}}(t)$, while the optical gain $g(z, t)$ in the SOA remains what it is after the precedent passage of A and B, as described in the algorithms in [7] and [13], i.e., $g(z, t)$ is not reset to its initial state $g = g_0$. This simply reflects the fact that every time slot is occupied by a pulse in harmonic mode-locking. After $N \sim 100$ roundtrips in favorable conditions, two consecutive inputs will have the same amplitude distribution, $|A^{N+1}_{\text{in}}| = |A^N_{\text{in}}|$, the steady state is thus achieved; otherwise $|A^{N+1}_{\text{in}}| \neq |A^N_{\text{in}}|$ whatever N is, the mode locking will not happen. The results presented in the next section are obtained with $N = 200$.

C. Theoretical Verification

Recall that for an arbitrary signal $A(t)$

$$\begin{aligned} TB &= \sigma_t \cdot \sigma_\omega \\ \sigma_x &= \left\langle x^2 \right\rangle - \langle x \rangle^2 \, (x = t, \omega) \\ \left\langle x^n \right\rangle &= \frac{1}{E}\int_{-\infty}^{\infty} x^n I(x)dx \\ E &= \int_{-\infty}^{\infty} I(x)dx \end{aligned} \tag{8}$$

where $I(t) = |A|^2$ and $I(\omega) = |\tilde{\text{A}}|^2$ are the intensities in the time- and frequency domain, respectively. The integration limits in time $(-\infty, \infty)$ are replaced by $(0, T)$ for a periodic signal, and E is the signal's energy in one period. The integrations in (8), as well as in the following, are carried out using the 6th-order Bode's rule [14].

For an ideal Gaussian, TB = 1/2 and $\Delta\text{f}\Delta\text{t} = 2\ln(2)/\pi$ [1]. These two reference values could test the precision of the chain of calculation, including integration, FT, sampling rate, speed of convergence, and so on. We calculated that for an ideal Gaussian, $A_1 = \exp[-(t - t_0)^2/\tau_0^2]$

$$\text{TB} = 0.5 \pm 0.0002,\ \Delta\text{f}\Delta\text{t} = 0.44127 \pm 0.00005 \ \text{(Gaussian)}$$

where τ_0 and t_0 are arbitrary parameters. Compared with the exact values, the relative errors are $\sim 10^{-4}$. For a chirp-free soliton, $A_2 = \text{sech}[(t - t_0)/\tau_0]$, the results are

$$\text{TB} = 0.5236 \pm 0.0002,\ \Delta\text{f}\Delta\text{t} = 0.327 \pm 0.002 \ \text{(soliton)}$$

The larger fluctuation ($\sim 10^{-3}$) of a soliton's $\Delta\text{f}\Delta\text{t}$ is because there is no analytical function to estimate its spectral FWHM using least-squares fitting [14]. The method of interpolation has to be used, resulting in some uncertainty at 10^{-3} level. However, a less accurate estimate of $\Delta\text{f}\Delta\text{t}$ does not degrade the precision of the calculated pulse itself. Notice also that a chirp-free soliton's TB is higher than that of a chirp-free Gaussian, but the opposite is true for $\Delta\text{f}\Delta\text{t}$. This discordance between TB and $\Delta\text{f}\Delta\text{t}$ reveals the important fact that $\Delta\text{f}\Delta\text{t}$ is not a good enough measure for judging the overall cleanness of a signal.

The precision of the model in nonlinear regime could be tested by launching an ideal Gaussian into SOA, and then comparing the amplified pulse with the analytical result in [6]. Fig. 4(a) shows the result using a Gaussian of $\Delta\text{t} = 3$ ps and $E = E_{\text{sat}}$. Other parameters are indicated in the figure. Fig. 4(b) is the spectrum of the output pulse. As can be seen in Fig. 4(a), the shape of the calculated output pulse is seamlessly superposed with the analytical curve. The calculation error of the algorithm in this nonlinear regime is difficult to estimate, since the analytical curve itself involves integrations [6]. It is reasonable, however, to assume that the relative error in Fig. 4(a) is of the same order as in the evaluation of (8), since the method of integration is the same. Consequently, we will adopt 4 digits for TB and 3 digits for $\Delta\text{f}\Delta\text{t}$ in the following results.

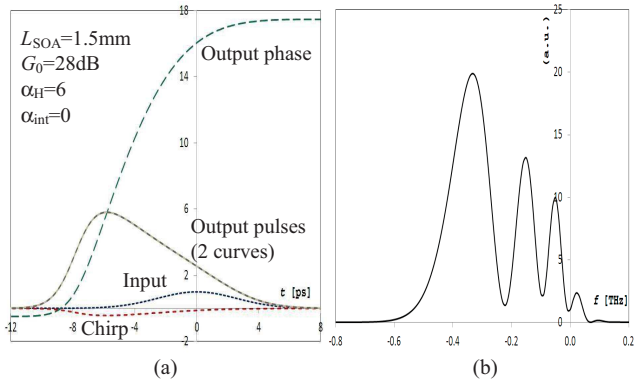

Fig. 4. Amplification of a 3-ps Gaussian pulse by SOA. (a) Input and the output pulses' intensities (analytical and calculation) in a linear scale, output pulse's phase in radian, and its chirp in THz. Notice that t is traced in a moving coordinate at the group velocity. (b) Spectrum of the output pulse.

The optical phase $\phi(t)$ of the output envelop has a "S" form, resulting in a nonlinear negative chirp, defined by $\delta f = -(2\pi)^{-1}\partial_t\phi$ in THz. The spectrum of this output pulse is highly distorted, as shown in Fig. 4(b). This output pulse has TB = 2.677, which is far higher than the Gaussian limit. Due to its multi-peak spectrum, its $\Delta f\Delta t$ is hardly meaningful and is not estimated.

It could be said, therefore, that the numerical procedures used in this paper are trustworthy; its predictions are in excellent agreement with available analytical results.

IV. Properties of Mode-Locked Pulses

The above algorithm is then applied to the experiment of Fig. 1, where the total fiber dispersion is estimated to be $DL = -25$ ps/nm; the filter bandwidth is $B_{BP} = 6$ nm; the average optical power injected into the rear facet is measured to be 9 mW, its peak intensity is therefore $B_0^2 \approx 23.5$ mW according to (6) with $\Delta_m = 0.7$. Substituting these values in the algorithm, mode-locking is obtained with $0.145 \leq \eta \leq 0.185$, which corresponds to a total transmission loss of $20\log_{10}\eta = -16.8 \sim -14.7$ dB outside SOA. With $\eta < 0.145$, the peak intensity of the output pulse will drop quickly below the noise level; if $\eta > 0.185$, the SOA output will be chaotic and there will be no mode locking. Fig. 5 shows the result obtained with $\eta = 0.152$, which corresponds most likely to the experimental observation of Fig. 2.

As can be seen in Fig. 5(a), the peak intensity of the output pulse $|A_{out}|^2_{max} = 12.5$ mW. After passing through an output coupler (80:20), an EDFA amplifier (9 dB) and a 50:50 power splitter, the peak intensity at the OSO in Fig. 1 should be $12.5 \times (0.2 \times 10^{9/10} \times 0.5) = 9.93$ mW. Taking into account some uncertainties, such as mode conversion loss between SOA and SMF, this value is in good agreement with the experimental result of 9.2 mW in Fig. 2. The calculated $\Delta f\Delta t = 0.459$, which is the same as experimental result (= 0.46).

Moreover, the calculated pulse's waveform and spectrum are both well fitted by Gaussians, as shown in Fig. 5. This is also the case for experimental results in [5]. Furthermore, the slight fluctuation around the output pulse's peak in Fig. 5(a) is indeed observed in Fig. 2, confirming once again the precision of the model and the algorithm, as well as the high resolution of the fast OSO. Notice also that the main peak in the spectrum is red-shifted of about −0.1 THz relative to the carrier frequency (at f = 0).

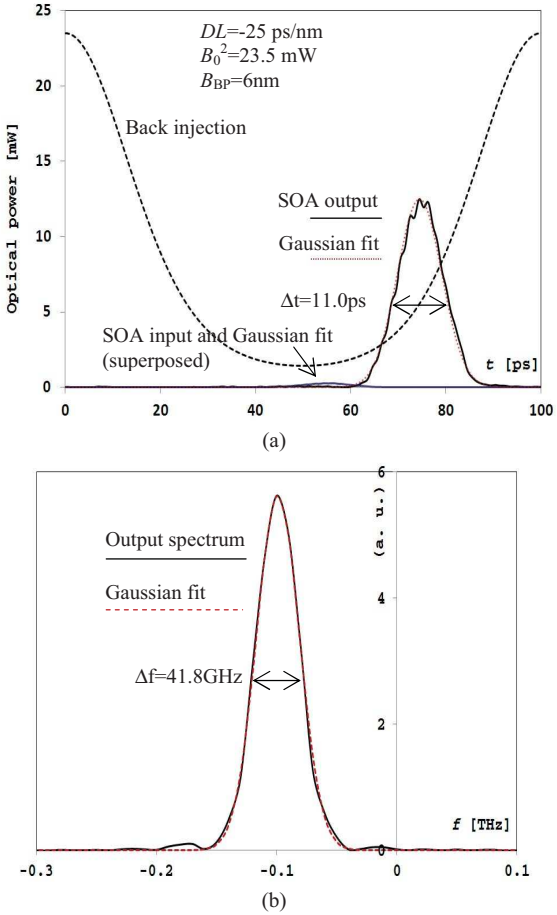

Fig. 5. Mode-locked pulse at $\eta = 0.152$. (a) Intensities of input pulses (two consecutive inputs totally superposed) measured at the front facet ($z = 0$), output pulse (with a Gaussian fit) and back injection intensities measured at the rear facet ($z = L_{SOA}$). The time shift between the input and the output pulses corresponds to the transmission delay in SOA. (b) Spectrum of output pulse with a Gaussian fit.

With its $\Delta f\Delta t = 0.459$, this output pulse is well qualified as transform-limited, even though some fluctuations can be observed in both its waveform and spectrum. However, it has TB = 2.526. This value is comparable to that obtained in Fig. 4, where severe distortions are clearly observed in both amplified pulse's waveform and spectrum.

As a matter of fact, the output pulse's waveform in Fig. 5(a) and its spectrum in Fig. 5(b) stretch widely below their half-maximum levels, resulting in the poor TB value above. These low-level fluctuations cannot be filtered out, however. By using a narrow-band filter (0.5∼1 nm) surrounding the main peak in Fig. 5(b), the pulse will change substantially its shape and spectrum, or simply collapse. This behavior is not revealed by its $\Delta f\Delta t$, in contrast to its TB. This issue will be further illustrated and discussed in the following examples.

Fig. 6 shows the output pulse's Δt, $\Delta f\Delta t$, TB, and its normalized peak power $|A_{out}|^2_{max}/B_0^2$ within the locking range. As can be seen in Fig. 6, the values of $\Delta f\Delta t$ within the

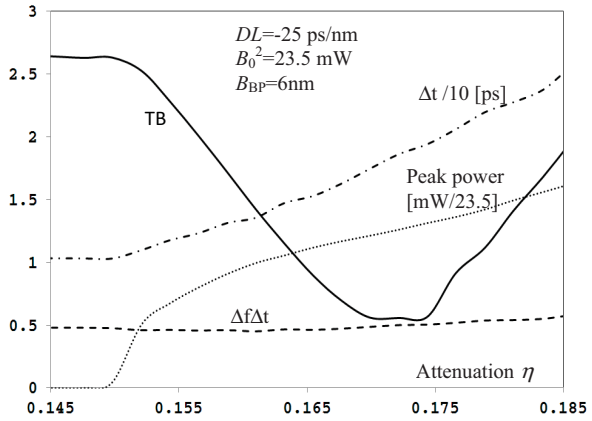

Fig. 6. Properties of mode-locked pulse at different cavity attenuation η. Pulse's width is divided by 10, its peak power is normalized to $B_0^2 = 23.5$ mW.

entire locking range remain very close to 0.5. Therefore, the output pulse is always transform-limited. In contrast, its TB varies strongly, with the minimum point TB = 0.5551 obtained at $\eta = 0.172$. At this point, the pulse has similar properties as those in Fig. 7 in terms of phase and chirp, and will be discussed together there. The fundamental Gaussian limit is thus still some distance away. It is not obvious to experimentally localize this minimum TB point using other, more measureable quantities as background. Notice also that, by adjusting the cavity loss, it is possible to obtain transform-limited pulses with a width $\Delta t = 10 \sim 25$ ps and a peak power of a few mW after the output coupler.

With $DL = -25$ ps/nm, as well as with other DL values used in the following, it is possible to obtain mode-locked pulses using other sets of parameters. In the above case of $DL = -25$ ps/nm, for example, the model predicts that mode-locking can happen with B_0^2 varying from a few tens of mW up to well beyond 100 mW, if $G_0 = 28$ dB and $B_{BP} = 6$ nm are maintained. However, an increasing B_0^2 reduces the effective SOA gain for mode-locked pulses, the cavity loss has to be reduced (η increased) to compensate the effect, as the model correctly predicts in agreement with physical insight. The problem of DCF-SMF link, mentioned in Section II, might then become a hurdle.

In order to further reduce the minimum value of TB = 0.5551 obtained with $DL = -25$ ps/nm, DL and B_0^2 are allowed to change in the simulation, while other parameters in Table 1 are kept unchanged. Fig. 7 shows the result obtained with $DL = -23.4$ ps/nm, $B_0^2 = 36.8$ mW and $\eta = 0.182$.

The output pulse in Fig. 7 has TB = 0.5086, which is very close to the fundamental Gaussian limit. It is even below that of an ideal hyperbolic secant (= 0.5236). The difference between the two values is well beyond the error margin in the calculation of TB. As a consequence, this pulse cannot be a soliton. Notice that this remark is based on TB, not on curve fitting or $\Delta f \Delta t$. (In effect, $\Delta f \Delta t = 0.327$ is never approached in our simulations).

From a theoretical point of view, only in the limit of slowly saturating gain, the master equation in [2] could become

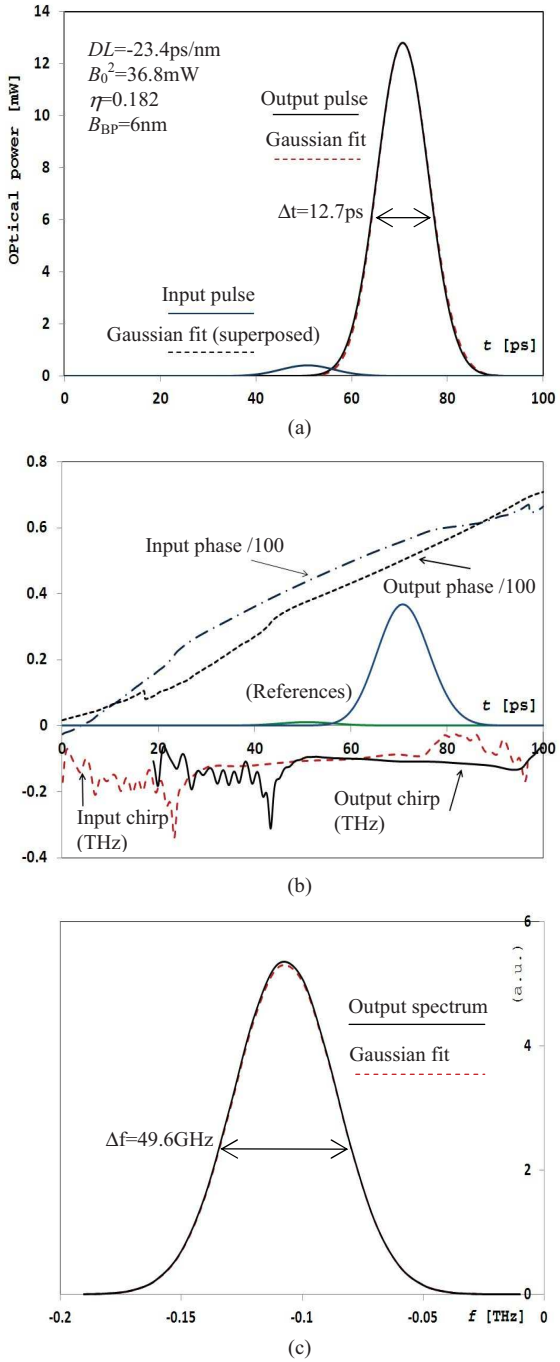

Fig. 7. Pulses obtained with $DL = 23.4$ ps/nm, $B_0^2 = 36.8$ mW, $\eta = 0.182$. (a) Input and output pulses' shapes and their Gaussian fits. (b) Correspondent optical phases (/100) in radian and chirps in THz. (c) Output spectrum with a Gaussian fit.

the nonlinear Schrödinger equation (NSE), whose solution is a soliton. This assumption is acceptable for erbium-doped fibers, where the carrier lifetime of $\sim$10 ms is far longer than the pulse widths [2]. In the case of SOA, however, the carrier lifetime is comparable to the pulse widths, this assumption is not true. In contrast, the master equation in [1] does not require the above condition. Instead, it applies the quadratic approximation, $\cos(\omega_m t) \approx 1 - (\omega_m t)^2/2$ around $t = 0$ in (7), which is usually acceptable around the trough

of the modulation function (see Fig. 5(a)). Unsurprisingly, SOA-related lasers such as this one would most likely support Gaussian pulses, if cavity dispersion is correctly adjusted.

Interestingly, the pulse in Fig. 7 is hardly transform-limited ($\Delta f \Delta t = 0.634$), even though both its waveform and spectrum are remarkably well fitted by Gaussians. Here, once again, TB and $\Delta f \Delta t$ deliver contradictory messages about the cleanness of a pulse.

The optical phases and chirps illustrated in Fig. 7(b) could help understand why this pulse has such a low TB. Contrary to the nonlinear "S" shape of the phase in Fig. 4(a), both input and output pulses in Fig. 7(b) have nearly linear phases during the time slots where the pulses' intensities are significant. As a consequence, their instantaneous frequencies (chirps) are nearly constant during the corresponding time slots. According to *Fourier Shift Theorem*, their spectra are simply red-shifted, as confirmed by Fig. 7(c). In effect, it is this nearly constant chirp which explains the cleanness of this pulse. Furthermore, a careful inspection of Fig. 7(b) reveals that the input and the output chirps have opposite slopes (upward for the input, downward for the output). This is the result of the dispersion management with DCF. In effect, the role of DCF in this ring laser is not to eliminate the spectral red-shift associated with SOA's amplification, but to smooth the pulse's phase so that the red-shift becomes nearly constant and therefore harmless regarding the cleanness of the pulse.

It is probable that the above TB = 0.5086 could be further reduced if G_0 and Δ_m are allowed to change as well. The interest of doing this seems limited, since it would not help gain more insight into the system.

It is also observed that the pulses in Figs. 5–7 are essentially unchanged to a varying B_{BP} between 5∼8 nm in the simulation, implying that the initial assumption of the carrier frequency ω_0 at the center of the filter is acceptable for these pulses, whose spectral spans are narrow compared to B_{BP}. Our simulation also shows that clean pulses (TB < 0.6 and $\Delta f \Delta t \sim 0.5$, say) can be expected in a range $DL = -23 \pm 3$ ps/nm by adjusting B_0^2 and η only (similar to Fig. 6). All these provide some margins for practical applications.

If the cavity dispersion DL deviates substantially from the above equilibrium point ($DL \sim -23$ ps/nm), however, the pulse's phase and chirp will become erratic, resulting in poor TB and misleading $\Delta f \Delta t$. A typical example is shown in Fig. 8, which is obtained with $DL = -10$ ps/nm, $B_0^2 = 27.9$ mW, $\eta = 0.206$ and, noticeably, $B_{\mathrm{BP}} = 5$ nm, which differs from previous cases ($B_{\mathrm{BP}} = 6$ nm).

The output pulse in Fig. 8(a) has a peak power of 24.8 mW and a relatively narrow width of $\Delta t = 6.90$ ps. It has complicated waveform and spectrum, resulting in TB = 10.31, a very poor value indeed. Meanwhile, its $\Delta f \Delta t = 0.426$, which paradoxically qualifies the pulse as transform-limited.

As shown in Fig. 8(b), the spectrum of this pulse is far more extended than previous cases of Figs. 5–7. As a result, the interaction of this pulse with the filter becomes important. In effect, the mode-locking cannot happen with $B_{\mathrm{BP}} = 6$ nm if other parameters are roughly the same as before. With the help of a narrower filter of 5 nm, the lower (red) end of the pulse's spectrum will be re-shaped and limited, as can be

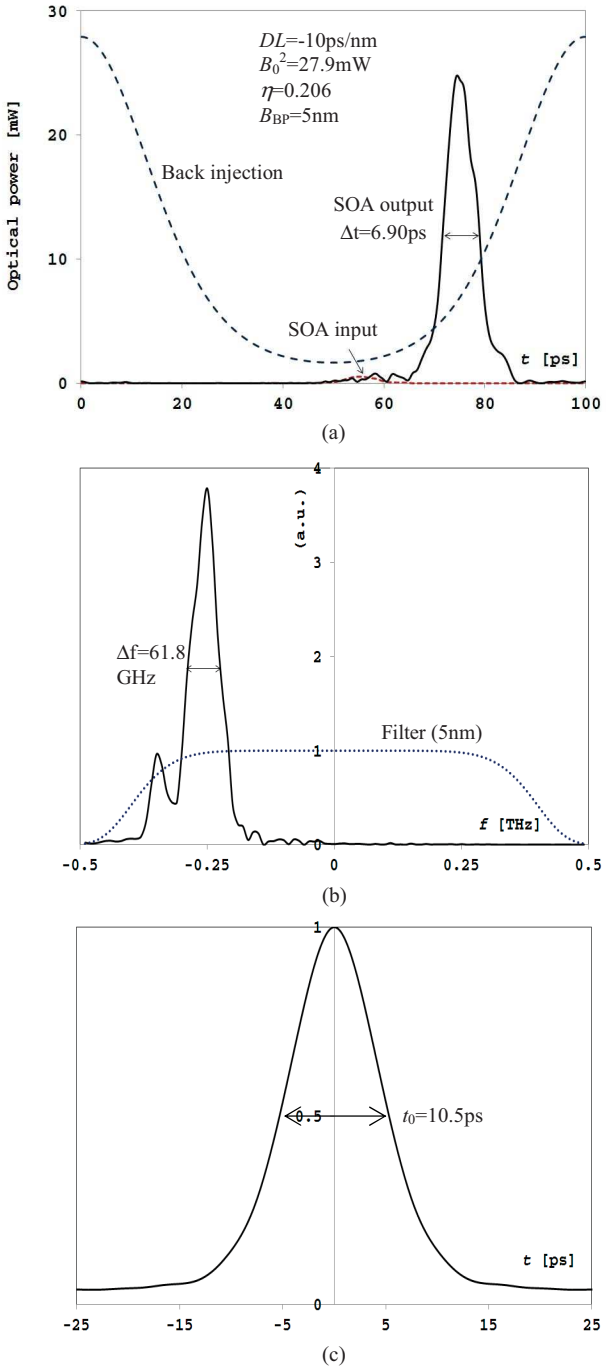

Fig. 8. Pulse obtained with $DL = 10$ ps/nm and $B_{\mathrm{BP}} = 5$ nm. (a) Input and output pulses' waveforms and the back injection. (b) Output pulse's spectrum and the filter function. (c) Calculated intensity autocorrelation trace of the output pulse.

seen between $f = -0.5 \sim -0.25$ THz in Fig. 8(b). Since the spectral energy is near zero on the other (bleu) side of the filter, a narrower filter is effectively equivalent to a red-shift of the carrier frequency ω_0 from the center of a wider filter. In other words, it is the spectral distance between ω_0 and the red-end of the filter that matters, as long as B_{BP} is wide enough. As a consequence of this interaction between the pulse and the filter, the filter bandwidth B_{BP} should be allowed to change or, alternatively, the carrier frequency ω_0

needs to be shifted, in order to obtain mode-locked pulses in the condition of unbalanced dispersion. To the authors' best knowledge, this "red-wall" effect, *i.e.*, the spectral re-shaping by the filter's red-end to stop pulses' excessive red-shift so as to maintain mode-locking, is not predicted before this study.

The second-order autocorrelation trace of the output pulse, calculated using *Wiener-Khinchin Theorem*, is shown in Fig. 8(c). It is remarkably clean, with the FWHM width $t_0 = 10.5$ ps. This corresponds to $\Delta t = 7.42$ ps if the initial pulse is supposed to be a Gaussian, or $\Delta t = 6.77$ ps if a soliton is assumed [16]. Both values are in good agreement with the original one. Meanwhile, all details of the original pulse are washed out. Were this pulse indeed produced in an experiment, and then measured by the usual autocorrelation technique, it would not be difficult to fit approximately the autocorrelation trace with both assumptions. As a consequence, conclusions or theories that follow might be unrealistic. Therefore, independent of theoretical models or laser systems which may produce such a pulse, its potential existence should not be ignored.

V. Conclusion

The model presented in this paper demonstrates its capability of predicting and analyzing the behaviors of mode-locked optical pulses in a SOA-fiber ring laser. The associated algorithm is shown to be accurate enough to address the questions asked at the beginning of the paper.

In the condition of adequate cavity dispersion, nearly perfect Gaussian pulses can be expected. Their time-bandwidth product using RMS definition could be very close to the fundamental Gaussian limit. These pulses would have a slight and linear chirp as a result of the dispersion management. Thanks to their narrow spectral widths, these pulses are resilient to parameter variations, including filter bandwidth change. If the cavity dispersion is not correctly adjusted, the cleanness of mode-locked pulses will degrade, as measured by their energy spreads in both time- and frequency domain. These pulses will then have rather complicated waveforms and spectra, and are consequently more sensitive to parameter variations.

It is also demonstrated that this SOA-fiber ring laser does not support optical solitons. The method and arguments developed in this paper could be applied to other similar laser systems using SOA as active devices.

The results obtained in this study highlight the inadequacy of $\Delta f \Delta t$, the time-bandwidth product using FWHM definition, as an objective criterion for judging the overall cleanness of a pulse. The correlation between the cleanness of a pulse and its $\Delta f \Delta t$ value is not as strong as usually expected. As a consequence, the tacit significance of *transform-limited pulse* seems questionable, as well as its widespread use today.

The above results and observations are inseparable with a careful evaluation of optical phase. It is not obvious how to reveal the details of these pulses using intensity-based approaches such as autocorrelation. Indeed, some questions might be asked as to what extent an autocorrelation trace could be used, and whether the curve-fitting is trustworthy enough to serve beyond a pure illustrative propose.

References

[1] A. E. Siegman, *Lasers*. Herndon, VA: Univ. Sci. Books, 1986.

[2] H. A. Haus, K. Tamura, L. E. Nelson, and E. P. Ippen, "Stretched-pulse additive pulse mode-locking in fiber ring lasers: Theory and experiment," *IEEE J. Quantum Electron.*, vol. 31, no. 3, pp. 591–598, Mar. 1995.

[3] L. Cohen, *Time-Frequency Analysis*. Englewood Cliffs, NJ: Prentice-Hall, 1995.

[4] J. H. Chung and A. M. Weiner, "Ambiguity of ultrashort pulse shapes retrieved from the intensity autocorrelation and the power spectrum," *IEEE J. Sel. Topics Quantum Electron.*, vol. 7, no. 7, pp. 656–666, Jul. 2001.

[5] A. Fernandez, C. Lu, and J. W. D. Chi, "All-optical clock recovery and pulse reshaping using semiconductor optical amplifier and dispersion compensating fiber in a ring cavity," *IEEE Photon. Technol. Lett.*, vol. 20, no. 12, pp. 1148–1150, Jul. 2008.

[6] G. P. Agrawal and N. A. Olsson, "Self-phase modulation and spectral broadening of optical pulses in semiconductor laser amplifiers," *IEEE J. Quantum Electron.*, vol. 25, no. 11, pp. 2297–2306, Nov. 1989.

[7] J. W. D. Chi, C. Lu, and M. K. Rao, "Time-domain large-signal investigation on nonlinear interactions between an optical pulse and semiconductor waveguides," *IEEE J. Quantum Electron.*, vol. 37, no. 10, pp. 1329–1336, Oct. 2001.

[8] G. P. Agrawal, *Lightwave Technology*. New York: Wiley, 2004.

[9] B. Edvold and L. Gruner-Nielsen, "New technique for reducing the splice loss to dispersion compensating fiber," in *Proc. ECOC Conf.*, 1996, pp. 245–248.

[10] G. P. Agrawal, "Effect of gain dispersion on ultrashort pulse amplification in semiconductor laser amplifiers," *IEEE J. Quantum Electron.*, vol. 27, no. 6, pp. 1843–1849, Jun. 1991.

[11] M. Y. Hong, Y. H. Chang, A. Dienes, J. P. Heritage, P. J. Delfyett, S. Dijaili, and F. G. Patterson, "Femtosecond self- and cross-phase modulation in semiconductor laser amplifiers," *IEEE Select. Topics Quantum Electron.*, vol. 2, no. 3, pp. 523–539, Sep. 1996.

[12] G. P. Agrawal, *Nonlinear Fiber Optics*. San Francisco, CA: Academic, 2005.

[13] J. W. D. Chi, A. Fernandez, and C. Lu, "A comprehensive modeling of wave propagation in photonic devices," *IET Commun.*, vol. 6, no. 5, pp. 571–576, 2012.

[14] W. H. Press, S. A. Teukolsky, W. T. Vetterling, B. P. Flannery, *Numerical Recipes*. Cambridge, U.K.: Cambridge Univ. Press, 1992.

[15] C. M. D. Sterke, K. R. Jackson, and B. D. Robert, "Nonlinear coupled equations on a finite interval: A numerical procedure," *J. Opt. Soc. Amer. B*, vol. 10, no. 3, pp. 403–412, Mar. 1991.

[16] A. Yariv, *Optical Electronics in Modern Communications*. London, U.K.: Oxford Univ. Press, 1997.

Jacques W. D. Chi received the B.Eng. degree in electronic engineering from Tsinghua University, Beijing, China, in 1985, and the M.Sc. and Ph.D. degrees in optoelectronics from the Institut d'Electronique Fondamentale (IEF), University of Paris-11, Paris, France, in 1987 and 1991, respectively.

He was an Assistant Professor with the Ecole Natioanle d'Ingénieurs de Brest (ENIB), Brest, France, in 1991, where he is currently an Associate Professor with the Maître de Conférences Hors Classe and Habilitation pour Diriger la Recherche. His current research interests include photonics, including nonlinear optics, semiconductor device modeling, and optical communication technology.

Dr. Chi is a member of the Société Française d'Optique.

Arnaud Fernandez was born in Albi, France, in 1979. He received the Masters degree in electronic engineering from the National Engineering School of Brest, Brest, France, in 2003, and the M.Sc. and Ph.D. degrees from the Université de Bretagne Occidentale, Brest, in 2004 and 2009, respectively. His doctoral research focused on theoretical and experimental research of intracavity dispersion management in an active mode-locked laser using a semiconductor optical amplifier in a fiber ring cavity, was expanded to the application of such laser device in an all optical clock-recovery scheme.

He joined the MOST Group, LAAS-CNRS, in 2012, as an Assistant Professor.

Chao Lu (M'91) received the B.Eng. degree in electronic engineering from Tsinghua University, Beijing, China, in 1985, and the M.Sc. and Ph.D. degrees from the University of Manchester, Manchester, U.K., in 1987 and 1990, respectively.

He was with the School of Electrical and Electronic Engineering, Nanyang Technological University, Singapore, from 1991 to 2006. From 2002 to 2005, he was with the Institute for Infocomm Research, Agency for Science, Technology and Research, Singapore, as the Program Director and the Department Manager. He joined the Department of Electronic and Information Engineering, The Hong Kong Polytechnic University, Hong Kong. SAR, in 2006, as a Professor, where he is currently a member of the Photonic Research Centre and is involved in optical communication systems and fiber devices for communication and sensing systems.